ELSEVIER

Soil & Tillage Research 57 (2000) 13–30

Soil & Tillage Research

www.elsevier.com/locate/still

Drying of some Philippine and Indonesian puddled rice soils following surface drainage: Numerical analysis using a swelling soil flow model

J.M. Kirby*, A.J. Ringrose-Voase

CSIRO — Land and Water, GPO Box 1666, Canberra, ACT 2601, Australia

Received 16 March 1999; received in revised form 5 January 2000; accepted 5 June 2000

Abstract

Heavy clay soils used for paddy rice production in SE Asia are usually puddled to grow the rice crop. Soil conditions following puddling and drying might be unsuitable for following dry season crops, such as mungbean or soybean, which often produce poor or erratic yields. We analysed water movement in the drying process in order to better understand the drying behaviour in order that we may generalise the findings, and to examine the prospects for using a swelling soil flow theory in predicting that behaviour. A numerical solution to a general, material coordinate-based, one-dimensional flow equation for swelling soils was used to analyse experimental results from four sites in Indonesia and the Philippines. The soils at the four sites were a Ustic Epiaquert, a Typic Ustropept, an Aeric Tropoquept and a Chromic Epiaquert. In the experiments, evaporation, cracking and changes to moisture ratio (ratio of volume of moisture to volume of solid) and void ratio were monitored for several weeks following surface drainage. Hydraulic properties were also measured.

The numerical predictions of changes to moisture ratio compared well to the measured results. Predictions of cracking were based on assumptions about the ratio of vertical to lateral shrinkage, and reasonable comparisons were obtained with the measurements. The analysis showed that the measurement of soil evaporation by mini-lysimeters provided a good estimate of the overall soil evaporation at the wet end but underestimated evaporation from dry soil. The analysis also showed that the measurements of void ratio in the experiments were sometimes in error, because of difficulties in accurate volume sampling of very weak, wet soils. It is shown that in these swelling systems it was better to use material coordinates and moisture ratios rather than spatial coordinates and volumetric moisture contents.

Keywords: Swelling soils; Rice soils; Drying; Numerical modelling; SE Asia

1. Introduction

Heavy clay soils used for paddy rice (*Oryza sativa* L.) production in SE Asia are usually puddled to grow the rice crop. Soil conditions following puddling and drying might be unsuitable for following dry season crops, such as mungbean (*Vigna radiata* L. Wikz) or soybean (*Glycine max* L. Merr.), which often produce poor or erratic yields. As part of a wider investigation into management of puddled rice soils for dry season crops (So et al., 2000), Ringrose-Voase et al. (2000) used several field experiments to investigate the drying behaviour, including changes to physical and hydraulic properties of the soil. Here we analyse their experi-

* Corresponding author. Tel.: +61-2-6246-5921; fax: +61-2-6246-5965.
E-mail address: mac.kirby@cbr.clw.csiro.au (J.M. Kirby).

0167-1987/00/$ – see front matter
PII: S0167-1987(00)00131-8

ments using a numerical model of fluid flow in saturated–unsaturated swelling soil. Our aim is twofold: firstly, to better understand the behaviour of the soils in the experiments in order that we may generalise the findings, and secondly, to investigate the application of the flow model to puddled rice soils.

Several water balance and water flow models have been applied to rice soils, often as part of a rice growth or yield model. Water balance models (e.g., Burt et al., 1981; Radulovich, 1987; Chopart and Vauclin, 1990) are used to calculate the amount of water in the soil profile using empirical expressions for evapotranspiration. They do not account for the distribution of water in the profile, nor for the volume changes. The only water flow model that seems specifically to have been applied to rice soils is the SAWAH model (ten Berge et al., 1992, 1995) which uses a finite difference solution to Richards' equation together with a rice crop model. The soil is considered to be rigid, so volume changes are ignored. Ringrose-Voase et al. (1996) used SWIM, also based on Richards' equation, to model the drying of bare rice soil following surface drainage and harvest of the rice crop, though they recognised the rigid soil approach was an approximation. Clearly, many rice soils exhibit swell/shrink properties: they crack significantly upon drying, for example. Heavy clay soils used for rice occupy considerable areas. Smiles (1997) pointed out that using a rigid soil approach for a swelling soil problem might involve significant balance errors. Therefore, it is desirable to use a swelling soil solution for many puddled rice soils.

The flow equation for unsaturated swelling soils was derived by Philip (1969). The space coordinate, z, of the rigid soil equation is replaced by a material coordinate, m, and the resulting equation is similar in form to Richard's equation. Giraldez and Sposito (1985) solved a simplified, ψ-based (where ψ is the water potential) form of the equation using an implicit finite difference technique. They used the solution to examine the ponding behaviour of unsaturated swelling soils. Kim et al. (1992) also solved a simplified, ψ-based form of the equation, using a Newton–Raphson solution technique, to analyse the flow and volume change behaviour during drying of soft marine sediments. Garnier et al. (1997a) solved the full ϑ-based (where ϑ is the volume of water per unit volume of solid, analogous to the volumetric moisture content, θ) form of the equation and Garnier et al. (1997b) developed an inverse method to derive the material hydraulic properties from test data. They also incorporated expressions, based on the work of Bronswijk (1990), that describe the division of volume change in an unrestrained soil between the vertical and the horizontal. In this paper, we apply a numerical solution to the swelling soil flow equation to analyse the experiments of Ringrose-Voase et al. (2000).

2. Numerical method for fluid flow in unsaturated swelling soil

The flow equation for unsaturated swelling soils is conveniently cast in a material distance, m, which is the length of solid traversed in a vertical direction, irrespective of the amount of pore space traversed. It is defined by

$$\mathrm{d}m = \frac{\mathrm{d}z}{1+e} \tag{1}$$

where z is the vertical distance in real space and e the void ratio (volume of void, including any void that appears as cracks, divided by volume of solid). It is also convenient to define the moisture ratio, ϑ, as

$$\vartheta = \theta(1+e) \tag{2}$$

where θ is the volumetric moisture content. With these definitions, the continuity equation is

$$\frac{\partial \vartheta}{\partial t} = \frac{\partial v}{\partial m} + S \tag{3}$$

where t is the time, v the velocity of flow of moisture relative to the solid (see Smiles, 1986) and S a source or sink. Darcy's law in a swelling system is

$$v = -\frac{k(\vartheta)}{(1+e)}\frac{\partial \phi}{\partial m} \tag{4}$$

where $k(\vartheta)$ is the moisture ratio-dependent hydraulic conductivity and ϕ the potential. The potential comprises the matric potential ψ, the gravitational potential z and the overburden potential

$$\phi = \psi - z + \alpha \int_0^M \gamma(1+e)\,\mathrm{d}m \tag{5}$$

where the final term on the right-hand side is the overburden potential due to the weight of soil above

the point in question, γ the wet density of the soil and α is related to the swelling characteristic of the soil (Philip, 1970). In Eq. (5), any load applied to the soil surface is ignored, since that is not a factor in the experiments described here. We shall here assume that α is approximated by $\mathrm{d}e/\mathrm{d}\vartheta$ (i.e., the change in volume with change in moisture ratio which, in a one-dimensional system, is also the change in height with change in moisture ratio and is independent of the overburden pressure) and further that $\mathrm{d}e/\mathrm{d}\vartheta$ is a constant. Ignoring the influence of the overburden on the swelling characteristic is common practice and might not be crucial (e.g., Philip, 1970). The relationship between the void ratio and moisture ratio measured in the field is often linear and so the second of these approximations is reasonable.

The gradient of the total potential is obtained by differentiating (5) with respect to m, noting (1) and the result is substituted into Darcy's law (4) to obtain

$$v = -k_{\mathrm{m}} \frac{\partial \psi}{\partial m} + k^* \tag{6}$$

in which

$$k_{\mathrm{m}} = \frac{k(\vartheta)}{1+e}, \qquad k^* = k_{\mathrm{m}}(1+e)\left(1 - \frac{\mathrm{d}e}{\mathrm{d}\vartheta}\gamma\right) \tag{7}$$

in which k_{m} is a material coordinate hydraulic conductivity. It is now convenient to introduce a finite difference nomenclature and define v_- as the velocity between the points i and $i-1$ and v_+ as the velocity between the points i and $i+1$. Hence

$$v_+ = -k_{m_+} \frac{\psi_{i+1}^+ - \psi_i^+}{\Delta m_+} + k_+^*,$$
$$v_- = -k_{m_-} \frac{\psi_i^+ - \psi_{i-1}^+}{\Delta m_-} + k_-^* \tag{8}$$

in which ψ^+ indicates that the potentials are those at time $t + \Delta t$, $k_{m_+} = \frac{1}{2}(k_{m_{i+1}} + k_{m_i})$ and similarly for k_{m_-}, k_+^*, and k_-^*. Eq. (3) is rewritten as a non-linear difference equation

$$F = (v_+ - v_-) - (\vartheta_i^+ - \vartheta_i)\frac{\Delta m_i}{\Delta t} + S\,\Delta m_i \tag{9}$$

in which ϑ^+ is the moisture ratio at time $t + \Delta t$. The equation is a mixed form of flow equation, which is solved for $F = 0$. A non-linear Newton–Raphson method gives a fast and accurate solution (Ross, 1990; Kim et al., 1992).

In order to apply this theory, it is necessary to know the relationship between the moisture ratio and the potential, $\vartheta(\psi)$, the hydraulic conductivity and the potential, $k(\psi)$, and the relationship between moisture ratio and height change, $\mathrm{d}e/\mathrm{d}\vartheta$. In addition, the boundary conditions and the initial conditions, of ϑ, ψ and e, must be known.

3. Methods and materials

3.1. Soils and experiments

At four sites, two in the Philippines and two in Indonesia, the soil was flooded, puddled and sown to rice. At harvest, the soils were drained (i.e., the surface water was removed) and allowed to dry by evaporation while being kept free of weeds. The soils and the experiments were described in detail by Ringrose-Voase et al. (2000), with some further information on the soils given by Schafer and Kirchhof (2000). Here we give only a brief summary.

The experiments were conducted at four sites on soils chosen with a range of clay content and shrink–swell characteristics (Table 1). At San Ildefonso, Bulacan Province, in the Philippines, the soil was a Chromi-Hydragric Vertisol (Hypereutric) (ISSS/ISRIC/FAO, 1998) (Ustic Epiaquert in Soil Taxonomy, Soil Survey Staff, 1992). The surface soil had the least clay (35–40 g kg^{-1} <2 μm) and modified linear shrinkage ($\mathrm{LS}_{\mathrm{mod}}$) was 0.071, using the method of McKenzie et al. (1994) ($\mathrm{LS}_{\mathrm{mod}}$ is measured on air-dry soil ground to <2 mm and then wet to a potential of −100 cm $\mathrm{H_2O}$, whereas standard linear shrinkage is measured on a paste of remoulded soil). At Manaoag, Pangasinan Province, in the Philippines, the soil was a Hypereutric Cambisol (ISSS/ISRIC/FAO, 1998) (Typic Ustropept, Soil Survey Staff, 1992). The soil had a clay content of 500–550 g kg^{-1} <2 μm and $\mathrm{LS}_{\mathrm{mod}}$ was 0.096. At Maros, S Sulawesi, Indonesia, the soil was a Paraplinthi-Anthraquic Gleysol (Hypereutric) (ISSS/ISRIC/FAO, 1998) (Aeric Tropoquept, Soil Survey Staff, 1992) with a clay content was also 500–550 g kg^{-1} <2 μm, but was dominated by less shrink–swell minerals and so $\mathrm{LS}_{\mathrm{mod}}$ was only 0.050. The final site, at Ngale, near Ngawi, E Java, Indonesia, was a Grumi-Pellic Vertisol (Hypereutric) (ISSS/ISRIC/FAO, 1998) (Chromic Epiaquert, Soil Survey

Table 1
Particle size distributions, proportions (on whole soil basis) of swelling clay minerals and linear shrinkage for the soils of the four experimental sites (from Ringrose-Voase et al., 2000)

Site depth (cm)	Whole soil (g kg^{-1})				LS_{mod}[a]
	Sand (50–2000 μm)	Silt (2–50 μm)	Clay (<2 μm)	Smectite+Vermiculite	
San Ildefonso (Chromi-Hydragric Vertisol (Hypereutric))					
0–11	330	250	420	260 ± 80	0.071
11–30	340	170	490	340 ± 100	
Manaoag (Hypereutric Cambisol)					
0–7	10	430	560	480 ± 140	0.096
15–22	20	430	550	470 ± 140	
30–37	20	440	540	460 ± 140	
Maros (Paraplinthi-Anthraquic Gleysol (Hypereutric))					
0–12	20	490	490	150 ± 70	0.050
12–18	30	440	530	160 ± 70	
18–37	40	430	530	160 ± 70	
Ngale (Grumi-Pellic Vertisol (Hypereutric))					
0–15	60	160	780	740 ± 220	0.192
15–25	20	160	820	780 ± 230	
25–40	30	150	820	780 ± 230	

[a] Measured using the method of McKenzie et al. (1994).

Staff, 1992) and had the greatest clay content (800 g kg^{-1} <2 μm) and was the most shrink–swell, with LS_{mod} at 0.192.

At San Ildefonso, Maros and Ngale, the experiments were all conducted immediately following drainage of the surface water of the rice crop. The rice crop was removed immediately after drainage. At Manaoag, however, the experiment was conducted some time after the rice crop, and so the site was re-flooded and re-puddled prior to the experiment. This soil was particularly in a loose and wet condition at the start of the experiment, so much so that normal undisturbed coring was impossible as the soil flowed from the core.

3.2. Field measurements during the drying experiments: moisture content, etc.

For 4–6 weeks following drainage of the surface water, during which the experiments were kept free of vegetation, Ringrose-Voase et al. (2000) measured the moisture contents, density and moisture potentials at six depths in the soil in five replicated plots at each site. The first measurements were taken 1 day after surface drainage, except at Maros where they were taken 4 days after drainage. Subsequent measurements were taken at intervals of a few days.

On each sampling day soil moisture content, air-filled porosity and bulk density were measured using a single 10 cm diameter core taken from each of the five plots using a long coring tube and an electric jack hammer. The moisture potentials were measured using arrays of tensiometers installed at the six depths sampled for moisture content and density. Measurements were also taken of the length, depth and width of cracks.

Ringrose-Voase et al. (2000) also measured the loss of water by evaporation at the surface from 'mini-lysimeters', one in each of the five replicated plots. These were soil cores taken from the soil surface and isolated from the surrounding soil by plastic wrapping, but free to evaporate at the surface, and recovered a few days later to determine the weight loss. This was done several times throughout the experiment. The measurements of the moisture content change between sampling dates, together with the surface flux (evaporation) estimation and the moisture potential measurements, were sufficient to enable direct estimation using Darcy's law of the unsaturated hydraulic conductivity from the

moisture fluxes and hydraulic gradients (Ringrose-Voase et al., 2000). Although five measurements of moisture content and potential were taken at each depth for each sampling day, the measurements of the two variables were not taken at the same locations and so only the mean of the five values for each depth was used for the moisture and hydraulic conductivity estimates.

At San Ildefonso, Manaoag and Maros, rainfall and pan evaporation data were collected during the experiments. At all three sites, the evaporation estimated from the mini-lysimeters was initially about the same as pan evaporation and later reduced to less than pan. There was no effective rainfall at Manoaoag or Ngale, but at San Ildefonso about 11 mm fell at about the 20th day after drainage and at Maros there were two wet periods, on the eighth day and between the 23rd and 26th days. At Ngale, the pan evaporation was not measured.

3.3. Hydraulic properties of the four soils

Samples were taken (10 cm diameter cores, using a long coring tube and an electric jack hammer) from each of the five plots and used for laboratory measurement of the moisture characteristics of the soils, using a combination of tension and pressure plates (McIntyre, 1974). These, together with the field measured hydraulic conductivities, define the hydraulic properties of the soils. The van Genuchten relationship (van Genuchten, 1980) was fitted to the data using the RETC program (van Genuchten, 1978)

$$\frac{\vartheta - \vartheta_r}{\vartheta_s - \vartheta_r} = \frac{1}{(1 + (\beta\psi)^n)^m} \tag{10}$$

where β, n and m are empirical coefficients. (Note, van Genuchten (1980) used α in place of the β used in Eq. (10); we use β because α was used above and in the literature to denote a volume change property.) The equation was developed for volumetric moisture content data in rigid soils, but provided a good fit to the current moisture ratio data.

The material coordinate hydraulic conductivity relationships were also fitted to an equation due to van Genuchten (1980), but modified for moisture ratios

$$k_m = k_{ms} S_e^{1/2} (1 - (1 - S_e^{1/m})^m)^2 \tag{11}$$

where $S_e = (\vartheta - \vartheta_r)/(\vartheta_s - \vartheta_r)$, and ϑ_r and ϑ_s are, respectively, the residual moisture ratio and the moisture ratio at a suction of zero. In fitting this equation, the coefficients n and m were those found by fitting Eq. (10), so the shape of the curve was fully defined by the moisture characteristic; only the material coordinate hydraulic conductivity at zero suction, k_{ms}, was varied in fitting (11), so as to minimise the sum of squares of deviations between the line and values for k. Eqs. (10) and (11) are usually applied to rigid soils in terms of the volumetric moisture content, θ.

The relationship between moisture ratio and height change, $de/d\vartheta$ was not measured in the experiments. The measurements resulted in many data of void ratio, e, and moisture ratio, ϑ, but the scatter was too great to use for estimating $de/d\vartheta$. We assumed that $de/d\vartheta$ was equal to 0.3 for the Ngale soil. For the other soils, we assumed that their values as a proportion of 0.3 were in the same ratio as the LS_{mod} of the soil to the LS_{mod} of the soil at Ngale. Jayawardane and Greacen (1987) reported field measurements of $de/d\vartheta$ that varied from 0.119 to 0.320, and Talsma (1977) reported values that varied from 0.07 to 0.29. Jayawardane and Greacen (1987), reviewing both their own measurements and others reported in the literature, concluded that less than normal shrinkage (i.e., $de/d\vartheta$ less than 0.33) is the usual state of affairs, with the actual shrinkage depending on various factors including clay content. Our assumptions about $de/d\vartheta$ of the various soils are consistent with these conclusions.

3.4. Simulations performed

For each soil, two series of simulations were performed. The first was a simulation of the drying of the whole profile for the whole of the experimental period. At San Ildefonso, the field profile descriptions showed that the surface soil was underlain by a heavier clay at 70 cm, so we simulated the behaviour in only the top 70 cm. At the other sites, the profiles were uniform, and we simulated the behaviour in the top 150 cm. The simulations were performed using the material depths that corresponded to these actual depths. The initial conditions, at the time the surface water was drained, were estimated from the wettest profile encountered in the measurements.

The second series of simulations was of the behaviour in the mini-lysimeters. The depth assumed in the

simulation was the same as that of the cores used in the experiment and varied from 5 to 10 cm. Again, the equivalent material depths were used. Several simulations were performed in this series for each soil with a simulation for each mini-lysimeter drying event. These simulations were run for various periods from 1 to 8 days, with the periods being set to equal those for drying of the mini-lysimeters in the field experiments.

The mini-lysimeters were 5 or 10 cm deep cores taken at the surface on various days after the start of the experiments, which were then sealed at the base and installed back in the soil. Cores taken later in the experiment were generally drier than those taken earlier, except at Maros where it rained frequently. Thus, the initial conditions of ϑ and e in the mini-lysimeters varied with time in the experiments. The initial conditions used in the mini-lysimeter simulations were estimated from the predictions of ϑ, e and ψ of the profile simulations, for depths corresponding to the mini-lysimeter core.

3.5. Boundary conditions: profile simulations

At Maros, a water table was measured and was about 70–80 cm below the surface for most of the period after the 12th day. The bottom boundary at 150 cm for this site was assumed to be at a fixed potential of +60 cm. Standpipes were also installed at the other sites to measure the water table, but no water was found in them: there were either no water tables or they were deeper than the standpipes. (Note that this implies that the surface pond drained at the start of the experiment was a perched water table, perhaps sitting on the puddled layer.) Therefore conditions at the bottom boundary were not known at any of the other sites, so fixed potential boundaries were assumed.

At the top boundary, evaporation and rainfall were treated as a sink term (cf. Eq. (9)). The evaporation flux was calculated according to the scheme described by Campbell (1985) and used in SWIM (Ross, 1990; Verburg et al., 1996), in which the evaporation, E, is given by

$$E = E_{\mathrm{p}} \frac{h - h_{\mathrm{a}}}{1 - h_{\mathrm{a}}} \tag{12}$$

in which E_{p} is the potential evaporation and h_{a} the relative humidity of the air, assumed to be equal to 0.5 (as used in SWIMv1; see Verburg et al., 1996). The relative humidity at the soil surface, h, is a function of the soil water potential at the surface

$$h = \exp\left(\frac{M_{\mathrm{w}} \psi g}{RT}\right) \tag{13}$$

in which M_{w} is the mass of a mole of water (0.01802 kg/mol), g the gravitational constant (981 $\mathrm{cm^2/s}$), R the gas constant (8.3143×10^4 $\mathrm{cm^2/(s^2\ mol\ K)}$) and T the absolute temperature (K).

In Eqs. (12) and (13), the parameters are constants except for the soil water potential, ψ, which is calculated in the solution, and the potential evaporation, E_{p}. E_{p} was taken as the pan evaporation values measured at all the sites except Ngale. At the other three sites, the actual evaporation measured in the mini-lysimeters was equal to the pan evaporation for the first few days. Therefore, we assumed that at Ngale the pan evaporation was equal to the actual evaporation from the mini-lysimeters on the first day, and remained constant throughout the experimental period.

3.6. Boundary conditions: mini-lysimeter simulations

The mini-lysimeter cores were wrapped in plastic, except at the top where they were free to evaporate. Therefore, the bottom boundary was set to a no flow condition and the top boundary was treated as described above for the profile simulations.

4. Results

4.1. Hydraulic properties of the soils

The moisture and hydraulic conductivity characteristics of the four soils are shown in parts (a) and (b) of Figs. 1–4. Both characteristics showed considerable scatter, partly due to variation between samples or between locations in the field at which the moisture potential was measured, but also due to the difficulty of obtaining reliable moisture content and density samples in very soft, puddled soil. At San Ildefonso, Maros and Ngale, the field measurements of the moisture ratio, ϑ, and potential, ψ, showed great variation, so the laboratory measurements were used to define the moisture characteristic, $\vartheta(\psi)$ (Figs. 1a, 3a

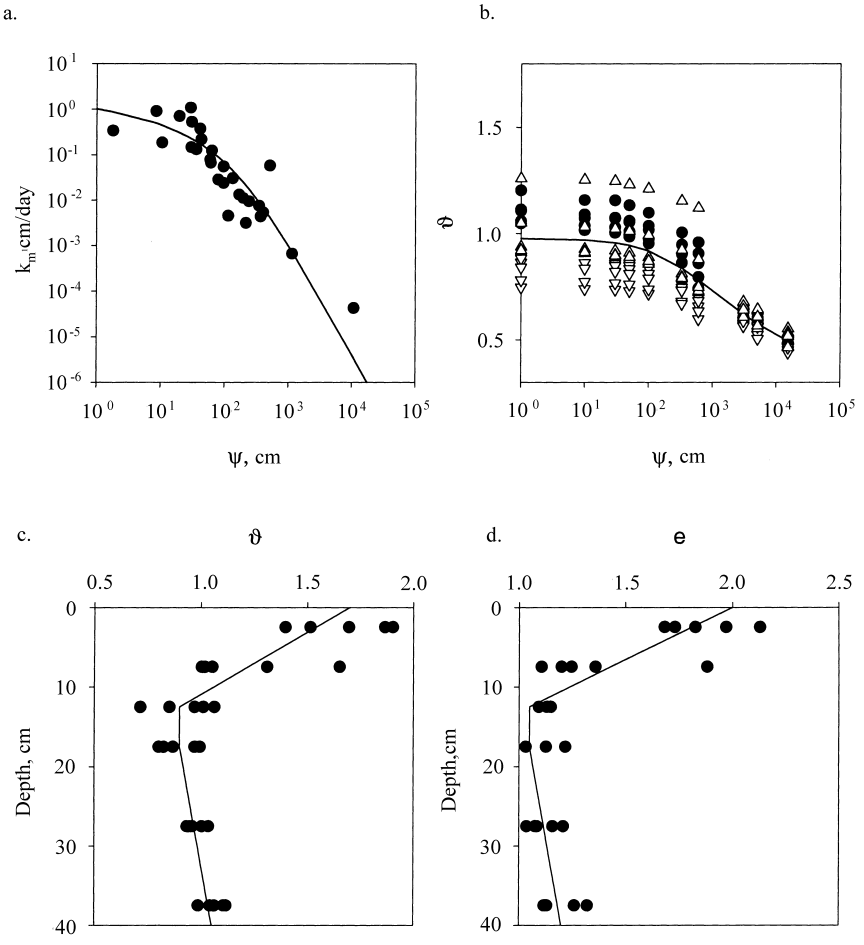

Fig. 1. Soil hydraulic properties and initial profile at San Ildefonso. (a) Relationship between material coordinate unsaturated hydraulic conductivity and soil water potential; points are measurements and line is fitted by the van Genuchten formula, Eq. (11). (b) Relationship between moisture ratio and soil water potential; points are measurements (filled circles, 0–5 cm depth; downward pointing triangles, 15–20 cm depth; upward pointing triangles, 30–35 cm depth) and line is fitted by the van Genuchten formula, Eq. (10). (c) Initial moisture ratio profile; points are measurements and line is the depth function assumed in the numerical analysis. (d) Initial void ratio profile; points are measurements and line is the depth function assumed in the numerical analysis.

and 4a). At Manaoag, however, there was less scatter in the field data and these were used instead (Fig. 2a).

The shape parameters in Eq. (10) (i.e., β, m and n) were similar (not significantly different) for all the layers sampled at a site. Therefore, these parameters were estimated by fitting Eq. (10) to the data for all sampled layers together. The coefficients of Eqs. (10) and (11) for the four soils are given in Table 2. The fitted lines are shown in Figs. 1a and b-4a and b. It should be noted that the values of k_{ms} in Table 2 are greater than those implied in Ringrose-Voase et al. (2000); the latter, however, resulted from fitting a different equation to the hydraulic conductivity data alone, with a much smaller slope at low suction, implying a smaller k_{ms}. The values of $de/d\vartheta$ are also shown in Table 2.

In the wettest profiles measured in the field at San Ildefonso, Maros and Ngale (Figs. 1c, 3c and 4c), particularly in the upper parts of the profile, ϑ was different from ϑ_s measured in the laboratory (cf. Figs. 1a, 3a and 4a). We assumed that ϑ_s for each layer in the analysis was given by the line fitted

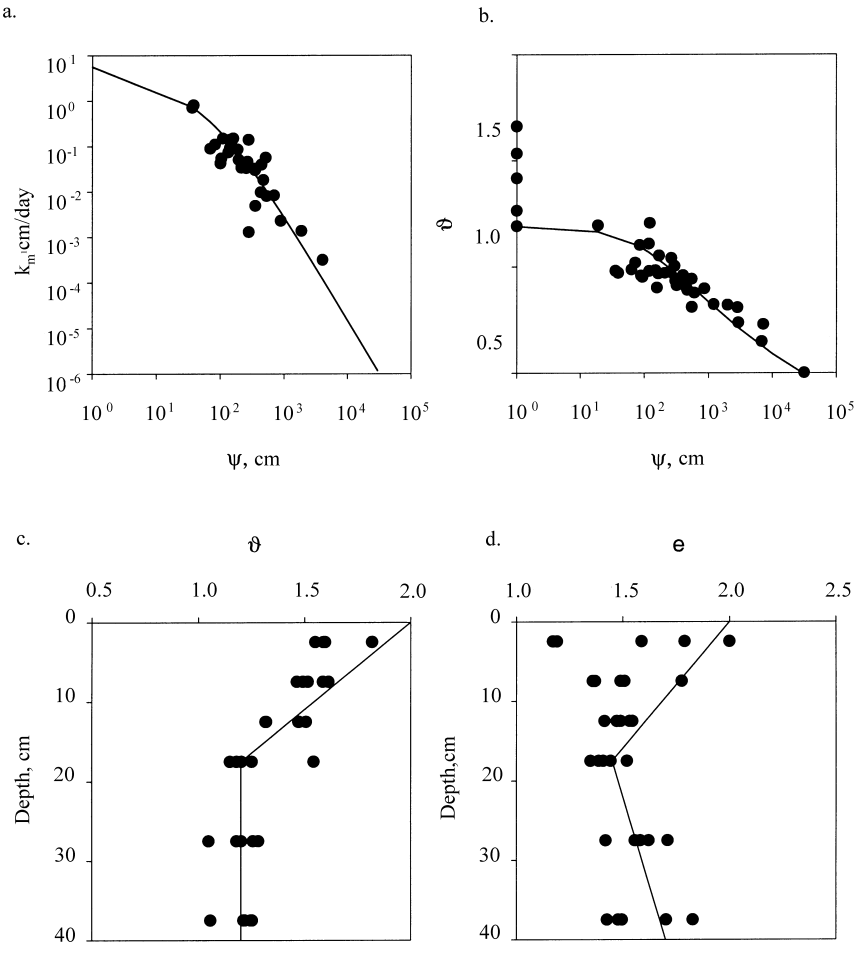

Fig. 2. Soil hydraulic properties and initial profile at Manoaoag. (a)–(d) Symbols and lines are the same as for Fig. 1, except in (b), where the symbols refer to all depths.

through the profile values on the wettest day (Figs. 1c, 3c and 4c). This is equivalent to assuming that the moisture characteristic in the soil profile has the same shape at all depths but the size is scaled with depth and hence overburden. This is reasonable in swelling soils that are flooded and puddled every year. The profile at Manaoag was treated somewhat differently, as explained in the following section.

4.2. Initial conditions of the soil profiles

The moisture ratio, ϑ, and void ratio, e, values measured at various depths for these wettest profiles are shown in parts (c) and (d) of Figs. 1–4. At Ngale and San Ildefonso, the wettest profile measured was on the first day. At Maros, the wettest profile occurred on the ninth day after rain on the eighth day. The relationships between depth, and ϑ and e for these profiles were estimated using linear interpolation between the measured means at each depth as shown in parts (c) and (d) of Figs. 1, 3 and 4. As noted above, the values of ϑ on this day were also used as ϑ_s for each layer.

At Manaoag, the wettest profile was that measured on the first day after drainage. We believe the soil might have consolidated in the early stages and so we assumed that the initial profile was a little wetter than is suggested by the measurements, as is shown by the straight line relationships between depth, and ϑ and e

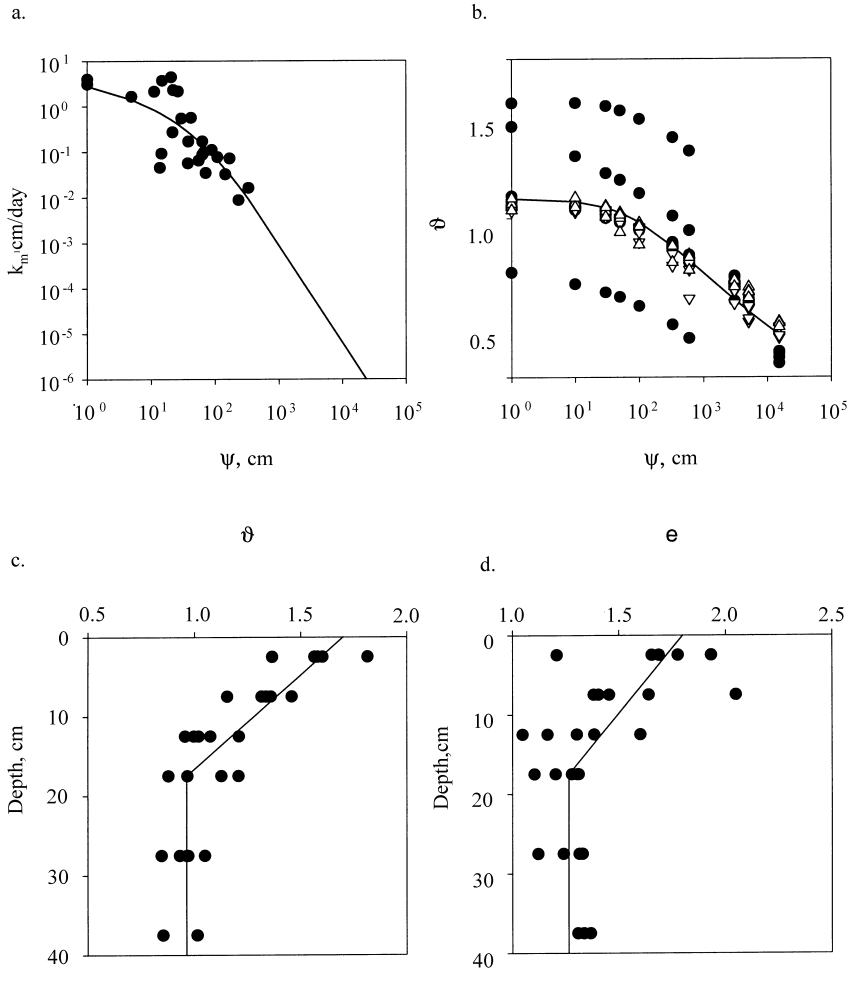

Fig. 3. Soil hydraulic properties and initial profile at Maros. (a)–(d) Symbols and lines are the same as for Fig. 1.

in Fig. 2c and d. We further assumed that during this early consolidation phase, the value of ϑ_s reduced linearly with increasing ψ until at $\psi = 19$ cm, and $\vartheta_s = 1.2$. There were three reasons for these assumptions. Firstly, this was the soil that was flooded and puddled immediately prior to drainage, and was very loose and wet and would be expected to consolidate under a small load. Secondly, the moisture characteristic (Fig. 2b) shows that four of the values of ϑ at $\psi = 1$ cm were wetter than the value ϑ_s of the line that best fitted the field $\vartheta - \psi$ data. These four values were measured on the first day and were not used to fit Eq. (10). At potentials of about 20 cm and greater, all the measured points are close to the best-fit line. Finally, numerical simulations of drying of this soil that used as the initial condition, the profiles shown in Fig. 2 resulted in poor comparisons between theory and experiment. Simulations based on a wet initial condition which consolidated to a drier value of ϑ_s at $\psi = 19$ cm were more satisfactory.

4.3. Evaporation at the surface

The evaporation rates predicted at the surface of the drying profile are shown in Fig. 5, together with the predictions and measurements for the mini-lysimeters. Rainfall and pan evaporation measurements (assumed in the case of Ngale) are also shown. No measure-

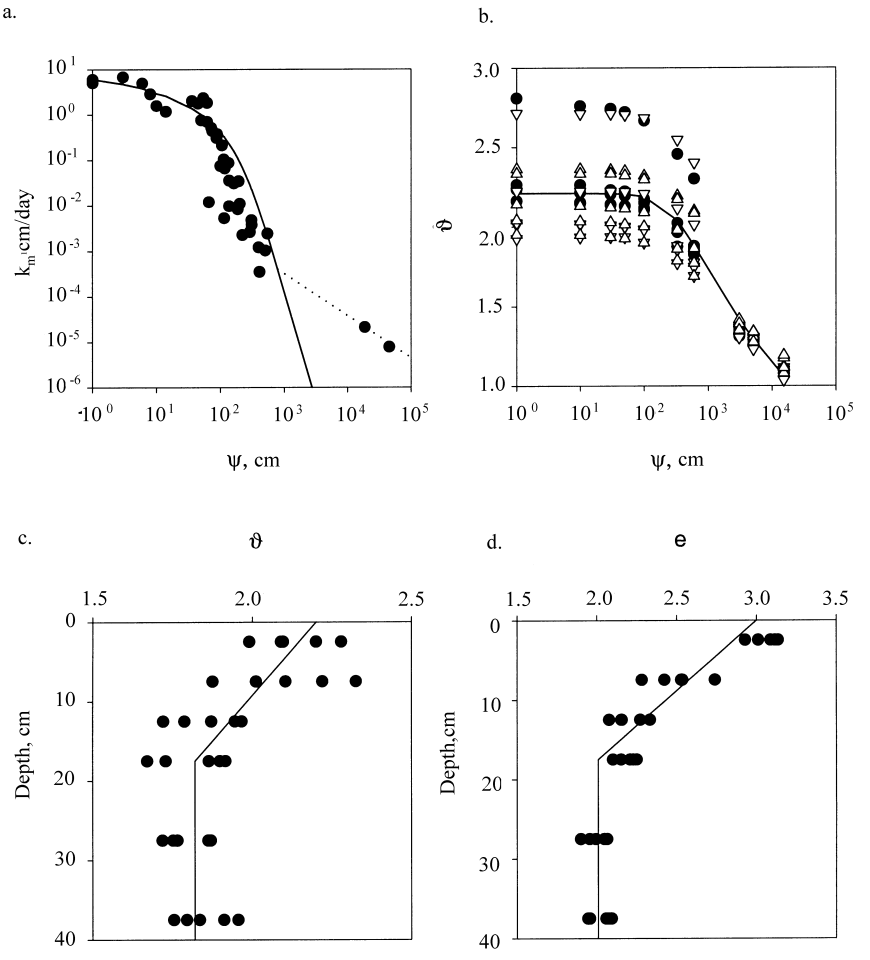

Fig. 4. Soil hydraulic properties and initial profile at Ngale. (a–d) Symbols and lines are the same as for Fig. 1.

ments were taken at Maros until the ninth day. So that the profile predictions can be compared to the mini-lysimeter predictions and measurements, the profile evaporation rates are shown averaged for the periods of drying of the mini-lysimeters. The rates predicted for the mini-lysimeters are less than those predicted for the whole profile, but the differences are generally not great. For Manaoag and Maros in particular, the

Table 2
Hydraulic property parameter values, void-ratio–moisture-ratio characteristic and bottom boundary condition used in the simulations[a]

Site	β	n	m	k_{ms} (cm/day)	$de/d\vartheta$	ψ at bottom boundary (cm)
San Ildefonso	0.0051	1.08	0.159	2.87	0.111	−200
Manaoag	0.0088	1.01	0.156	2.04	0.150	−1
Maros	0.0107	1.01	0.101	2.05	0.078	+70
Ngale	0.0038	1.21	0.082	1.51	0.300	−20

[a] β, n and m are the parameters in the van Genuchten equation (Eqs. (10) and (11)), k_{ms} the saturated hydraulic conductivity in material coordinates, $de/d\vartheta$ the change in volume with change in moisture ratio, and ψ the moisture potential.

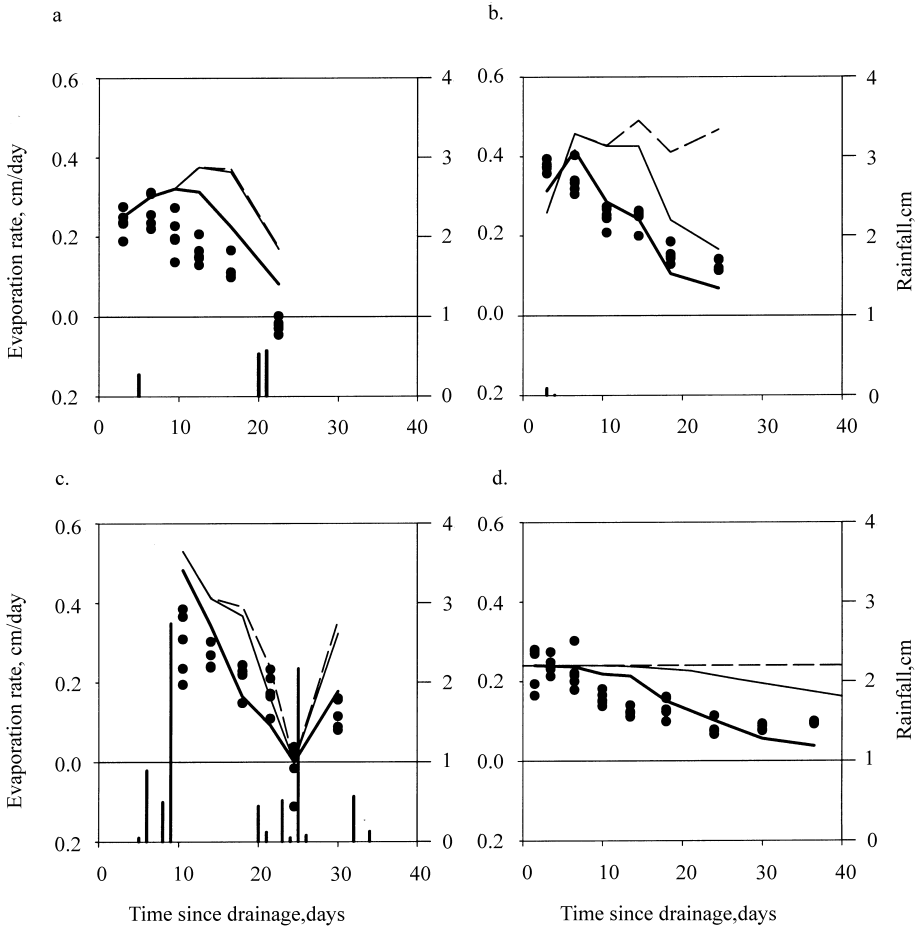

Fig. 5. Comparison of simulated and observed evaporation from mini-lysimeters and simulated evaporation from the profile. The thick and thin solid lines are the simulated evaporation from the mini-lysimeters and the whole profile, respectively; the points are the measurements from the mini-lysimeters; the broken lines are the measured pan evaporation, and the bars are the observed rainfall. (a) San Ildefonso; (b) Manaoag; (c) Maros; (d) Ngale.

rates predicted for the mini-lysimeters are stepped in the same fashion as the field measurements. The steps result from the interaction of the weather (rain and pan evaporation) and the different periods of drying between sampling days.

4.4. Moisture ratio profiles

It is usual to show the moisture ratio as a function of material depth, because areas under a curve in this space give a volume of water, such as the amount of water that has evaporated. However, the results presented by Ringrose-Voase et al. (2000) and other results discussed in this paper are given in terms of real depth. Therefore, for ease of comparison, the moisture ratio profiles are discussed in terms of real depth, but areas under curves do not give amounts of water.

The moisture ratio profiles on the first, last and an intermediate sampling day are shown in Fig. 6. It should be noted that at Maros, the profile was wetter on the intermediate sampling day (the ninth day after surface drainage) than on the first sampling day, due to rain on the eighth day. Although there are differences between simulated and measured profiles, the agreement is reasonable at all the sites.

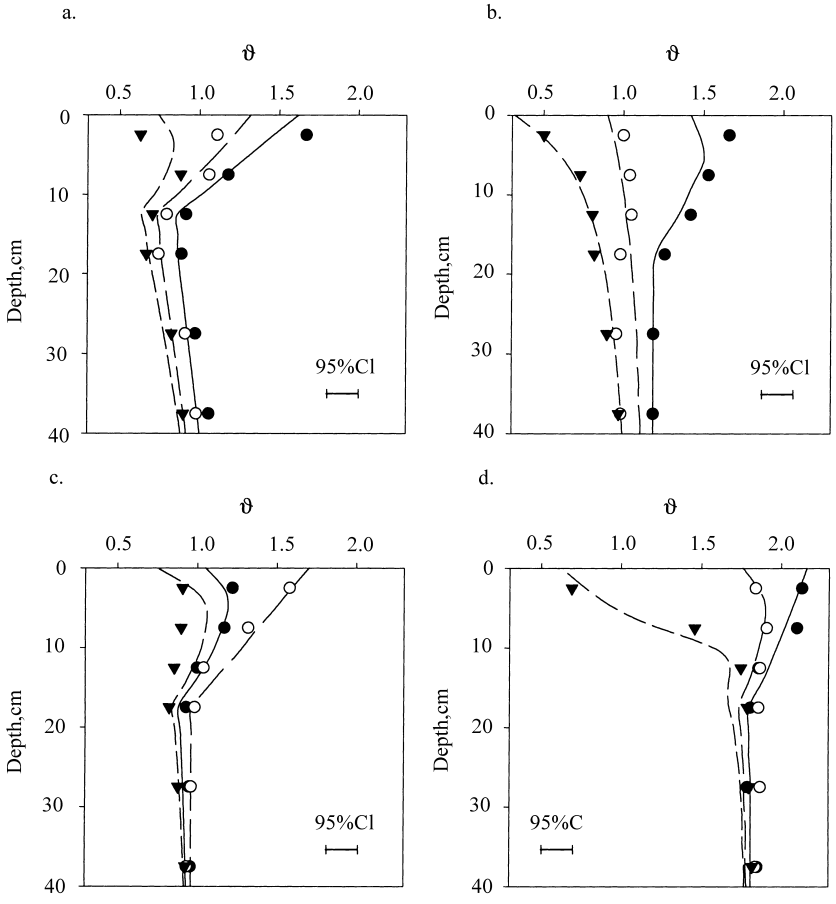

Fig. 6. Comparison of simulated and observed moisture ratio at three times. The lines are the simulated values and the points are the measured values. (a) San Ildefonso: filled circle represents day 1, open circle, day 8 and triangle, day 26 after drainage; (b) Manaoag: filled circle represents day 1, open circle, day 8 and triangle, day 28 after drainage; (c) Maros: filled circle represents day 4, open circle, day 9 and triangle, day 33 after drainage; (d) Ngale: filled circle represents day 1, open circle, day 8 and triangle, day 40 after drainage. The solid line represents the simulations for the first day (i.e., day 1 except Maros where it is day 4), the line with large dashes represent the middle day (i.e., day 8 except Maros where it is day 9), and line with the smaller dashes represent the last day (i.e., day 26, 28, 33 and 40, respectively). The bars represent the 95% confidence limits of the measured points.

4.5. Total void ratio profiles

The total void ratio is the ratio of all void space, both water and air filled, including void space due to cracks. The field measurements of density, based on samples taken between the cracks, had to be corrected for the estimated crack volumes to derive total void ratio (Ringrose-Voase et al., 2000). The simulated total void ratios are exactly those appearing in the theoretical equations in Section 2. The profiles are shown in Fig. 7. At Maros and Ngale, little change was measured during the course of the experiments, and this was matched by the predictions. At San Ildefonso and Manaoag, little change was predicted. However, the measurements indicate *increasing* void space as the profile dried. This seems physically impossible. We can think of no reasonably plausible mechanism that would result in a soil expanding on monotonic drying from a puddled and flooded condition. We assume that the measurements reflect from the difficulty of obtaining reliable volume samples in very soft soils. There might also be errors in estimation of the

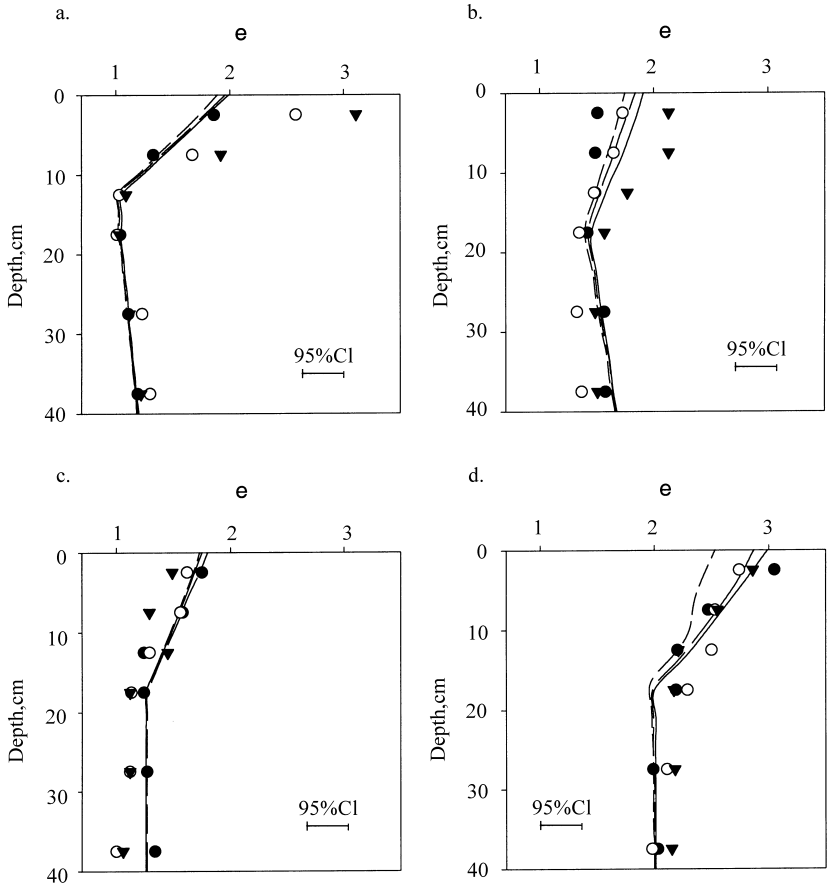

Fig. 7. Comparison of simulated and observed void ratio at three times. The void ratio is the total void space including cracks. (a)–(d) Symbols and lines are the same as for Fig. 6.

crack volume. At Manaoag in particular, the soil was soft enough in the early stage to be spooned into the sampling rings! Normal core sampling was impossible.

4.6. Profiles of void ratio between the cracks

The void ratio between the cracks is the ratio of all void space, both water and air filled, between the cracks and excludes void space in the cracks. The field measurements of density, based on samples taken between the cracks, were used directly to derive void ratio between the cracks. The simulated void ratios include the cracks and we have no direct information which we can use to calculate the partitioning of this void space into the cracks and the space between the cracks. However, with some simple assumptions we derived estimates of the partitioning. Cracking started immediately after drainage in the field, so we assumed that the volume change was approximately isotropic. The change in the simulated void ratio is equal to volume of settlement in a one-dimensional system. We assumed that the volume of cracks was twice the volume of settlement, which is a reasonable approximation to isotropic shrinkage when the settlement (or change in total void ratio) is small. This results in an estimate of crack volume at any depth equal to twice the volume due to predicted change in vertical length. Note that this is not part of the theory given in Section 2, but is a subsidiary calculation based on the assumptions about shrinkage and cracking. The crack volume so calculated was subtracted from the total volume and hence the void ratio between the cracks was estimated.

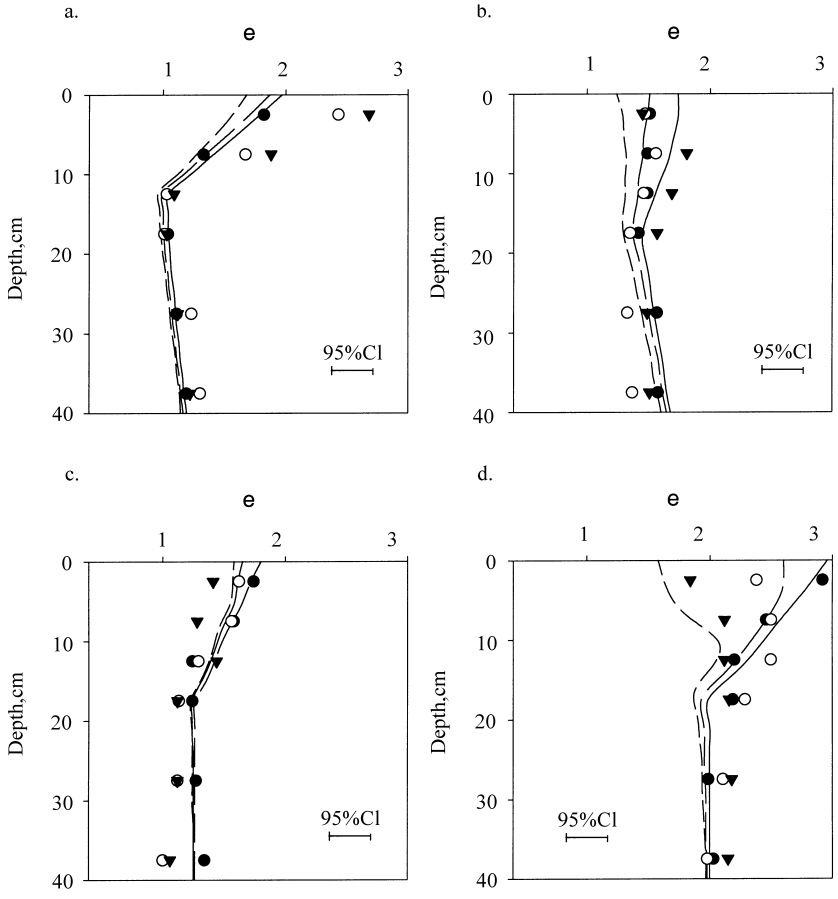

Fig. 8. Comparison of simulated and observed void ratio between the cracks at three times. (a)–(d) Symbols and lines are the same as for Fig. 6.

The profiles are shown in Fig. 8. At Maros and Ngale, the predicted and measured change in void ratio between cracks is small, but is greater than was the change in total void ratio (Fig. 7), as expected. Near the surface at Ngale, the measured and predicted change is greater, with void ratios roughly halving at the surface. At San Ildefonso and Manaoag, the measurements again indicate *increasing* void space as the profile dried, which again seems physically impossible.

4.7. Crack porosity profiles

The calculated crack volume described above was used to calculate crack porosity profiles (crack porosity is the fraction of the total volume occupied by cracks). Note again that this is a subsidiary calculation that is not part of the theory in Section 2. The measured and predicted profiles are shown in Fig. 9. The simulations predicted the greatest cracking at Ngale, intermediate at Manaoag and least at San Ildefonso and Maros. At all sites, the greatest cracking was predicted at the surface, and little at depth. These general features were similar to those observed. Differences between measurement and prediction might reflect inadequacies of the theory, but they might also result from measurement errors. The measurement technique provides only an estimate of the crack volume: the depth of cracks was estimated by poking a thin, flexible ruler into cracks, which gives a minimum estimate of the depth; the width of the cracks was measured directly at the surface, but the

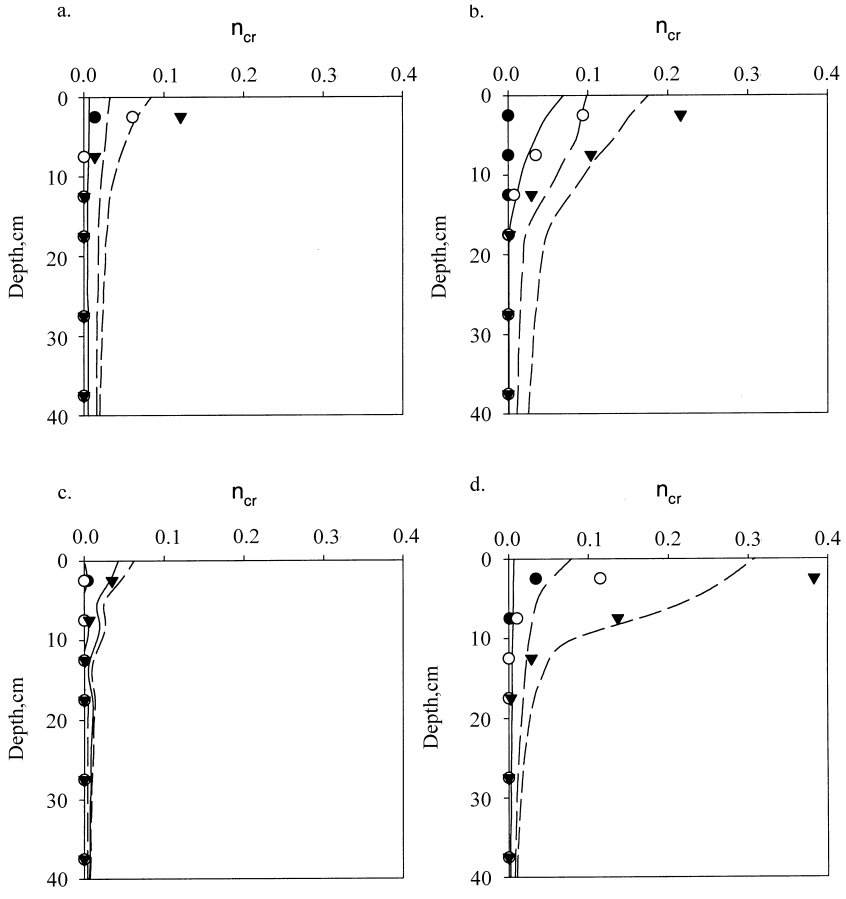

Fig. 9. Comparison of simulated and observed crack porosity at three times. (a)–(d) Symbols and lines are the same as for Fig. 6.

cross-sectional shape was simply assumed as triangular beneath the surface (Ringrose-Voase et al., 2000).

5. Discussion

5.1. Comparing the soils

The drying, cracking and volume changes in the four experiments were different. The differences were partly due to differences in soil properties and partly due to differences in experimental conditions.

All four soils showed greater drying near the surface than at depth, as would be expected (Fig. 6). All four also showed a change in drying behaviour at about 15 cm, which presumably indicates a compaction layer or ploughpan below the puddled layer. The heaviest clay with the smallest saturated hydraulic conductivity, k_s, and smallest unsaturated hydraulic conductivities, was at Ngale and little drying was observed or predicted below about 15 cm. The Manaoag soil had greater conductivities, and the profile was observed and predicted to dry noticeably to 40 cm depth. The drying at Manaoag was observed for only 26 days, compared to the 40 days at Ngale, so the difference is greater than it appears in Fig. 6. The behaviour at San Ildefonso, with intermediate conductivities, was observed and predicted to be intermediate between Ngale and Manaoag. Maros had the most permeable soil, but the two periods of rain prevented drying.

All four soils also showed the greatest volume change and cracking at the surface, with different behaviour below about 15 cm. The soil at Ngale had the greatest LS_{mod} and was both observed and predicted to show, near the surface, the greatest change in void ratio and greatest volume of cracking, and was observed and predicted to show little change in void ratio and little crack volume below about 15 cm. At Manaoag, the LS_{mod} was about half that of the Ngale soil, and the surface crack volumes were observed and predicted to be about half of those at Ngale. The San Ildefonso soil, with a smaller LS_{mod} than either Ngale or Manaoag, was observed and predicted to show smaller crack volumes than either of the other two. As discussed in Section 4, the observed changes to void ratio at San Ildefonso and Manaoag seem physically impossible. At Maros, the rain periods prevented much volume change or crack development.

5.2. Evaporation

The rate of evaporation from the soil surface at San Ildefonso, Manaoag and Maros was about the same as pan evaporation in the early stages (Fig. 5). The pan evaporation was not measured at Ngale, but it is reasonable to assume that, for the first few days, it was about equal to the soil evaporation. In the absence of other information, we assumed that it was constant throughout the experiment. In the later stages, the soil properties determine the actual evaporation. Therefore, we believe that the assumptions made for the Ngale soil are reasonable and will not greatly influence the prediction.

The calculation of hydraulic conductivities was based on estimating the fluxes and potentials in the field (Ringrose-Voase et al., 2000). The flux measurement was in turn based on measured changes to moisture content and estimated fluxes due to evaporation at the surface. The evaporative fluxes were estimated from the mini-lysimeters. Fresh surface soil was sampled and new mini-lysimeters were made on each sampling day, and it was assumed that the evaporation from a mini-lysimeter would not be significantly different to that from the surrounding soil in the few days before recovering and weighing the mini-lysimeter. However, the simulations show that this assumption is questionable at all four sites, because the predicted evaporation from the whole profile was greater than that from the mini-lysimeters. This in turn means that the estimated hydraulic conductivities might be in error. There is little error at the wet end, when rate of evaporation from both the whole profiles and mini-lysimeters was equal to pan evaporation. The error will increase with increasing drying.

The mini-lysimeter estimates of evaporation rate are nevertheless useful, as they enable the true soil surface evaporation to be bounded. The true rate must be equal to or greater than that estimated from the mini-lysimeters. Thus the true hydraulic conductivities at the dry end might be greater than those calculated. The true evaporation rate must also be equal to or less than pan evaporation. This provides a maximum possible estimate of the hydraulic conductivity at the wet end. The predicted evaporation rate from the whole profile was between these two extremes and might enable a better estimate of the evaporation than either of the bounds.

Based on these considerations, we suggest that mini-lysimeters and pan evaporation data can be used with an instantaneous profile method to estimate hydraulic conductivities. However, the estimates should be checked by analysis of the drying behaviour of the soil along the lines described in this paper. Errors are likely to be small or absent at the wet end but might be significant in drier soil.

5.3. Moisture ratios or moisture contents?

The theory of flow in unsaturated swelling soils outlined in Section 3 is most conveniently based on material coordinates and moisture ratios. There is also a practical advantage to using moisture ratios, particularly in the soft, puddled soils studied here. Sampling is difficult, and undisturbed sampling is virtually impossible until the soil has dried somewhat. Estimates of volume are likely to be in error, and hence volumetric moisture contents are likely to be poorly estimated. This appears to have happened at the San Ildefonso and Manaoag sites, where the apparent observed increases of void ratio (both total and between crack) during drying appear to be physically impossible. However, the water and solid do not separate during sampling and are likely to be sampled in the correct ratio. Thus the moisture ratio should provide a good estimate of the moisture conditions in the profile.

5.4. Estimates of cracks

The theory outlined in Section 2 is strictly one-dimensional, and contains information about void space but no information about cracks. A simple assumption about the way the void space was distributed enabled a subsidiary calculation about the volume of void that was expressed as a crack. This subsidiary calculation is similar to the methods of Bronswijk (1988) and Garnier et al. (1997a) (though they incorporated the assumptions into the one-dimensional flow theory) in estimating crack volumes and their relation to one-dimensional shrinkage, though here we use an approximate expression.

However, this is not a theory about cracks, nor does it explain the mechanism of cracking. There is no suggestion about the spatial arrangement or size of cracks, i.e., whether there are a few wide cracks or many narrow ones. Neither soil strength nor overburden were considered to play a part. It is likely that cracks would not open at depth where the overburden pressure due to the weight of the soil above would prevent horizontal shrinkage. A probable upper bound to the amount of void expressed as crack volume can be calculated, by assuming that shrinkage is normal (i.e., the soil shrinks by a volume equal to the volume of water extracted) and that all shrinkage that is not seen as a change of height is expressed as a crack. This is not a true upper bound because, in principle, soil could crack without settlement but this is unlikely. Therefore, it might be possible to gain insight into crack development and its relation to drying using this approach.

6. Conclusions

There was considerable variability in the data used to estimate the hydraulic properties $\vartheta(\psi)$ and $k(\psi)$. There was also uncertainty about the $\mathrm{d}e/\mathrm{d}\vartheta$ relationship and conditions at the lower boundary of the simulated profiles. In consequence, we do not regard the comparisons between predicted and observed profiles as evidence for verification of the theoretical equations or the numerical method. We have shown that differences between measurement and prediction were often a result of difficulties in the measurement or estimation of parameters in soft rice soils. Rather, our purpose was to use the analyses to provide insight into the experiments and into the drying behaviour of puddled rice soils. This, we believe, we have achieved. From the observations and analyses we conclude that

- the four soils behaved differently, partly because of the different initial conditions and the weather, but also because of their different hydraulic and shrink–swell properties;
- consolidation of very loose soil might be a mechanism responsible for some volume change in recently puddled soil and should be investigated further;
- the instantaneous profile method using mini-lysimeters to estimate evaporation rates provides a good estimate of hydraulic conductivities at the wet end, and a useful lower bound approximation at the dry end;
- it is advantageous to use moisture ratios and material coordinates rather than volumetric moisture contents;
- some insight into the relationship between crack development and drying might be gained from the type of analysis outlined here; and,
- the lower boundary condition should be estimated better than we were able to, perhaps by direct measurement of suctions and fluxes at some depth.

Finally, this study is part of a larger project examining the prospects of improving yields of dry season crops. It is, of course, impractical to examine the issues experimentally for all soil types in all areas, or for a sufficiently long period to determine the probability of events such as crop failure due to waterlogging as a result of heavy dry season rain. The unsaturated swelling soil flow theory and the numerical implementation used here can be adapted to examine the issues computationally. Notwithstanding the uncertainties, we regard the comparisons between theory and experiment as sufficiently encouraging to pursue this avenue. We shall report the results in another paper.

Acknowledgements

The experimental investigation was supported by the Australian Centre for International Agricultural Research (ACIAR). The authors thank the many

members of staff of the following organisations who helped with the field experiments: the Bureau of Soils and Water Management, Quezon City, The Philippines, the Research Institute for Maize and Other Non-rice Cereal Crops, Maros, Indonesia, the Faculty of Agriculture, Brawijaya University, Malang, Indonesia and the Research Centre for Food Legumes and Tuber Crops, Malang, Indonesia.

References

Bronswijk, J.J.B., 1988. Modelling of water balance, cracking and subsidence of clay soils. J. Hydrol. 97, 199–212.

Bronswijk, J.J.B., 1990. Shrinkage geometry of a heavy clay soil at various stresses. Soil Sci. Soc. Am. J. 54, 1500–1502.

Burt, J.E., Hayes, J.T., O'Rourke, P.A., Terjung, W.H., Todhunter, P.E., 1981. A parametric crop water use model. Water Resour. Res. 17, 1095–1108.

Campbell, G.S., 1985. Soil Physics with BASIC. Elsevier, New York.

Chopart, J.L., Vauclin, M., 1990. Water balance estimation model: field test and sensitivity analysis. Soil Sci. Soc. Am. J. 54, 1377–1384.

Garnier, P., Perrier, E., Angulo Jaramillo, R., Bavaye, P., 1997a. Numerical model of three-dimensional anisotropic deformation and one-dimensional water flow in swelling soils. Soil Sci. 162, 410–420.

Garnier, P., Rieu, M., Boivin, P., Vauclin, M., Bavaye, P., 1997b. Determining the hydraulic properties of a swelling soil from a transient evaporation experiment. Soil Sci. Soc. Am. J. 61, 1555–1563.

Giraldez, J.V., Sposito, G., 1985. Infiltration in swelling soils. Water Resour. Res. 21, 33–44.

ISSS/ISRIC/FAO, 1998. World reference base for soil resources. World Soil Resources Reports 84. FAO, Rome.

Jayawardane, N.S., Greacen, E.L., 1987. The nature of swelling in soils. Aust. J. Soil Res. 25, 107–113.

Kim, D.J., Diels, J., Feyen, J., 1992. Water movement associated with overburden potential in a shrinking marine clay soil. J. Hydrol. 133, 179–200.

McIntyre, D.S., 1974. Water retention and the moisture characteristic. In: Loveday, J. (Ed.), Methods for Analysis of Irrigated Soils. Commonwealth Bureau of Soils Technical Communication 54. Commonwealth Agricultural Bureaux, Farnham Royal, UK, pp. 43–62.

McKenzie, N.J., Jaquier, D.J., Ringrose-Voase, A.J., 1994. A rapid method for estimating soil shrinkage. Aust. J. Soil Res. 32, 931–938.

Philip, J.R., 1969. Hydrostatics and hydrodynamics in swelling soils. Water Resour. Res. 5, 1070–1077.

Philip, J.R., 1970. In: Youngs, E.G., Towner, G.D. (Eds.), Reply to Comments on 'Hydrostatics and Hydrodynamics in Swelling Soils'. Water Resour. Res. 6, 1248–1251.

Radulovich, R., 1987. AQUA, a model to evaluate water deficits and excesses in tropical cropping. Part I. Basic assumptions and yield. Agric. For. Meteorol. 40, 305–321.

Ringrose-Voase, A.J., Kirby, J.M., Gunomo, D., Sanidad, W.B., Serrano, C., Lando, T.M., 1996. Changes to the physical properties of soils puddled for rice during drying. In: So, H.B., Kirchhof, G. (Eds.), Management of Clay Soils for Rainfed Lowland Rice-based Cropping Systems. ACIAR Proceedings No. 70. ACIAR, Canberra, ACT, pp. 71–89.

Ringrose-Voase, A.J., Kirby, J.M., Gunomo, D., Sanidad, W.B., Serrano, C., Lando, T.M., 2000. Changes to the physical properties of soils puddled for rice during drying. Soil Till. Res., in press.

Ross, P.J., 1990. SWIM — A Simulation Model for Soil Water Infiltration and Movement. Reference Manual. CSIRO Division of Soils, Townsville, Qld.

Schafer, B.M., Kirchhof, G., 2000. Soils and climate. Project 8938: benchmark sites for lowland rice-based cropping systems. Soil Till. Res., in press.

Smiles, D.E., 1986. Principles of constant-pressure filtration. In: Cheremisinoff, N.P. (Ed.), Encyclopaedia of Fluid Mechanics. Gulf Publishing Company, Houston, TX, pp. 791–824.

Smiles, D.E., 1997. Water balance in swelling materials: some comments. Aust. J. Soil Res. 35, 1143–1152.

So, H.B., Ringrose-Voase, A.J., Utomo, W.H., Adisarwanto, T., Prastowo, B., Dacanay, E.V., Kirchhof, G., 2000. Rainfed lowland rice-based cropping systems: an overview. Soil Till. Res., in press.

Soil Survey Staff, 1992. Keys to Soil Taxonomy, 5th Edition. SMSS Technical Monograph No. 19. Pocahontas Press, Blacksburg, VI.

Talsma, T., 1977. Measurement of the overburden component of the total potential in swelling field soils. Aust. J. Soil Res. 15, 95–102.

ten Berge, H.F.M., Jansen, D.W., Rappoldt, K., Stol, W., 1992. The Soil Water Balance Module SAWAH Description and Users Guide. Simulation Monograph 22. DLO-CABO, Wageningen, the Netherlands.

ten Berge, H.F.M., Metselaar, K., Jansen, M.J.W., de. San Agustin, E.M., Woodhead, T., 1995. The SAWAH riceland hydrology model. Water Resour. Res. 31, 2721–2732.

van Genuchten, M.Th., 1978. Calculating the unsaturated hydraulic conductivity with a new closed-form analytical model. Research Report 78-WR-08. Department of Civil Engineering, Princeton University, Princeton, NJ.

van Genuchten, M.Th., 1980. A closed-form equation for predicting the hydraulic conductivity of unsaturated soils. Soil Sci. Soc. Am. J. 44, 892–898.

Verburg, K., Ross, P.J., Bristow, K.L., 1996. SWIMv2.1 User Manual. Divisional Report No. 130. Division of Soils, CSIRO.